since 1961

Baltica

BALTICA Volume 37 Number 2 December 2024: 24–38
https://doi.org/10.5200/baltica.2024.2.3

An evaluation of the earthquake potential with seismic and tectonic variables for the West Anatolian region of Türkiye

Serkan Öztürk*, Hamdi Alkan

Öztürk, S., Alkan, H. 2024. An evaluation of the earthquake potential with seismic and tectonic variables for the West Anatolian region of Türkiye. *Baltica 37(2)*, 110–124.Vilnius. ISSN 0067-3064.
Manuscript submitted 9 September 2024 / Accepted 23 October 2024 / Available online 28 November 2024

Abstract. In the present study, an evaluation of the region-time-magnitude behaviours of the earthquake occurrences in the West Anatolian Region (WAR), Türkiye, is carried out using the statistical and seismotectonic parameters such as the *b*-value of Gutenberg-Richter relation, occurrence probabilities, and return periods of earthquakes. We also have mapped the Coulomb stress changes to observe the current and future earthquake hazard. In recent years, several large earthquakes such as the 1919 Soma (Mw = 6.7) and the 2022 and 2024 Aegean Sea (Mw = 5.3 and Mw = 5.1) revealed earthquake potential in the WAR. Coulomb stress analyses of 41 local events with mostly normal fault mechanisms have shown that positive lobes (> 0.0 in bars) are mainly confined in the crust and uppermost mantle depths around Samos, Kos, and south of Lesvos. The smaller *b*-values (< 1.0) are observed in the same regions. On the contrary, we have observed a higher *b*-value from the offshore to onshore, south to north-trending direction, and negative scattered stress lobes (< 0.0 in bars) in slightly NW–SE oriented. The relationship between an increased *b*-value and negative stress change may indicate a similar seismicity for the region. In addition, we have analyzed the occurrence probabilities and return periods of the earthquakes, which showed us that Mw = 6.0 may occur at 75% in the intermediate term with an estimation of ~7 years. Our results reflect that these types of multiple-parameter assessments are important to define regional seismicity, seismic, tectonic, and statistical behaviours. Consequently, the areas with reductions in *b*-values and increments in stress imply the possible seismic hazard in the intermediate/long term.

Keywords: *The West Anatolian region; b-value; Coulomb stress; Seismic hazard*

*Serkan Öztürk** *(seko6134@gmail.com)* *https://orcid.org/0000-0003-1322-5164*
Department of Geophysics, Gümüşhane University, 29100, Gümüşhane, Türkiye
Hamdi Alkan (hamdialkan@yyu.edu.tr) *https://orcid.org/0000-0003-3912-7503*
Department of Geophysics, Van YüzüncüYıl University, 65080, Van, Türkiye

**Corresponding author*

INTRODUCTION

Many studies exist on the regional and temporal evaluation of earthquake potential and seismic hazard for active zones of Türkiye and the world. These determinations use different tools such as scaling laws, physical models, variables, etc. Therefore, if seismic and tectonic models of earthquake behaviours can be attributed to a statistical basis, these approaches will contribute to the estimation of the next possible earthquakes. There exist two types of approaches: (*i*) evaluation of experimental data based on the earthquake indicators (precursors) and (*ii*) statistical analysis of earthquake behaviours (Holliday *et al*. 2007). For this purpose, the most basic and often preferred scaling tools such as the *b*-value, standard normal deviate *Z*-value (precursory seismic quiescence), *Mc*-value (cut-off or completeness magnitude), *Dc*-value that describes the fractal dimension, occurrence probability and return period of earthquakes, time series

analyses of earthquakes and stress distributions are preferred in the earthquake statistic. Thus, there exist many different physical approaches and their applications for the evaluation of characteristics of earthquake behaviours and the estimation of future earthquake occurrences on the Earth (Kagan, Knopoff 1987; Matsumura 1993; Molchanov *et al*. 1998; Polat *et al*. 2002; Öncel, Wilson 2004; Console *et al*. 2007; Roy *et al*. 2011; Scholz 2015; Mousavi 2017; Çoban, Sayıl 2019; Öztürk 2020; Ulukavak *et al*. 2020; Akar 2021; Sinaga *et al*. 2022; Öztürk, Alkan 2023; Ormeni *et al*. 2023).

It is well-known that Türkiye is one of the most seismotectonically active parts of the Earth, and many studies have presented different perspectives to describe the earthquake characteristics and hazard for active zones. One of these most active regions is the West Anatolian Region (WAR), western Türkiye. This region has a significant earthquake potential in terms of the large earthquake occurrences from the past to the present. The nature and structure of the WAR show differences along the Hellenic arc. The eastern part of Hellenic presents a transform fault characteristic. In this zone, right and left lateral strike-slip faults striking the northeast-southwest and northwest-southeast directions are observed in and around the horst-graben systems. However, the active faults in the region are characterized mainly by normal faulting mechanisms (Aktuğ *et al*. 2009; Özer, Polat 2017a, b; Emre *et al*. 2018). The structures of the crustal and upper mantle of this region have a complex seismotectonic background. Hence, strong/large earthquakes occurred in the WAR from the historical period to the present. For example; 1919 Soma (Mw = 6.7, moment magnitude), 1928 Trbalı (Mw = 6.5), 1939 Dikili–Bergama (Mw = 6.6), 1949 Karaburun (Mw = 6.7), 1955 Söke–Balat (Mw = 6.7), 1969 Alaşehir (Mw = 6.7), 1992 Doğanbey (Mw = 6.1), 1995 Dinar (Mw = 6.2), and 2003 Seferhisar–İzmir (Mw = 5.7). Also, many medium/large earthquakes occurred in the Aegean Sea between 2017 and 2020 (Koeri 2024). Thus, we state that the WAR is a seismically and tectonically very complex region of Türkiye, and the most recent earthquakes mentioned above caused major disasters.

In this study, we achieved a comprehensive analysis for earthquake hazard evaluation by considering region-time-magnitude behaviours of seismicity in the WAR. Although several studies with different variables were supplied for this region, these applications associated with seismic and tectonic perspectives were comparably rare for this part of Türkiye. In this context, an appraisal of seismotectonic variables such as the *b*-value of the magnitude-frequency distribution of earthquakes and Coulomb stress changes are realized. Also, the return period and occurrence probability were estimated for the strong earthquake occurrences. The findings will not only be significant in terms of describing the seismic behaviour but also will contribute to the understanding of earthquake potential in the study area.

ACTIVE TECTONIC STRUCTURE IN THE WEST ANATOLIAN REGION

The geodynamic structure in the Mediterranean region, associated with the Alpine-Himalayan tectonic belt, originates from the collision of the Eurasian, Arabian, and African plates, which influences the west Anatolia-Aegean region by generating different types of deformation, along the Hellenic and Cyprian arcs with the Bitlis-Zagros Suture zone (BZSZ) (Bayrak *et al*. 2017; Över *et al*. 2021). Due to the N–S directional compression regime in the Eastern Anatolia, the collision tectonic is created between the Anatolian and Arabian plates. Therefore, the Anatolian plate shifted to the west along the North Anatolian Fault Zone (NAFZ) and the East Anatolian Fault Zone (EAFZ) (Oral *et al*. 1995; McClusky *et al*. 2000). This tectonic escape concludes with the N-S extensional tectonic regime shown in E–W horst-graben systems in the Aegean microplate and Western Anatolian Extension Province (WAEP) under the north–south extension (Dewey, Şengör 1979; Şengör *et al*. 1985). These horst-graben systems such as Gediz and Büyük Menderes are bordered by mainly normal faults in the north–south and the east–west directions (Över *et al*. 2021; Mulumulu *et al*. 2023; Çırmık *et al*. 2024). On the other hand, the African plate convergence towards the Anatolia plate causes the consumption of oceanic lithosphere along the Hellenic and Cyprus arcs (McClusky *et al*. 2000; Reilinger *et al*. 2006; Över *et al*. 2021). The Hellenic arc has a significant effect on the geodynamic process of the WAR. Subduction along the Cyprian and Hellenic arcs causes a convergence between Anatolian and African plates (Şaroğlu *et al*. 1992; Bozkurt 2001). These active tectonics and related deformations are followed by intense seismicity with many earthquakes in the region. This extensional zone is one of the most active seismotectonic structures of Türkiye (Fig. 1a). The tectonic map showing the major faults in the WAR is given in Fig. 1b (simplified and changed from Li *et al*. 2003 and Emre *et al*. 2018). The major tectonic structures in the study region can be given as Gülbahçe and Soma-Kırkağaç Fault Zones, Mordoğan, Seferhisar, Tuzla, Güzelhisar, Zeytindağ, Bergama, Efes and Milas faults, Gediz, Küçük and Büyük Menderes Graben Systems. According to geodetic measurements, the Aegean domain migrates an annual Global Positioning System (GPS) velocity of ~33 mm/yr to the SW with a N–NE movement of the African plate. The Anatolian plate rotates counter-clockwise at ~18–25 mm/yr (Reilin-

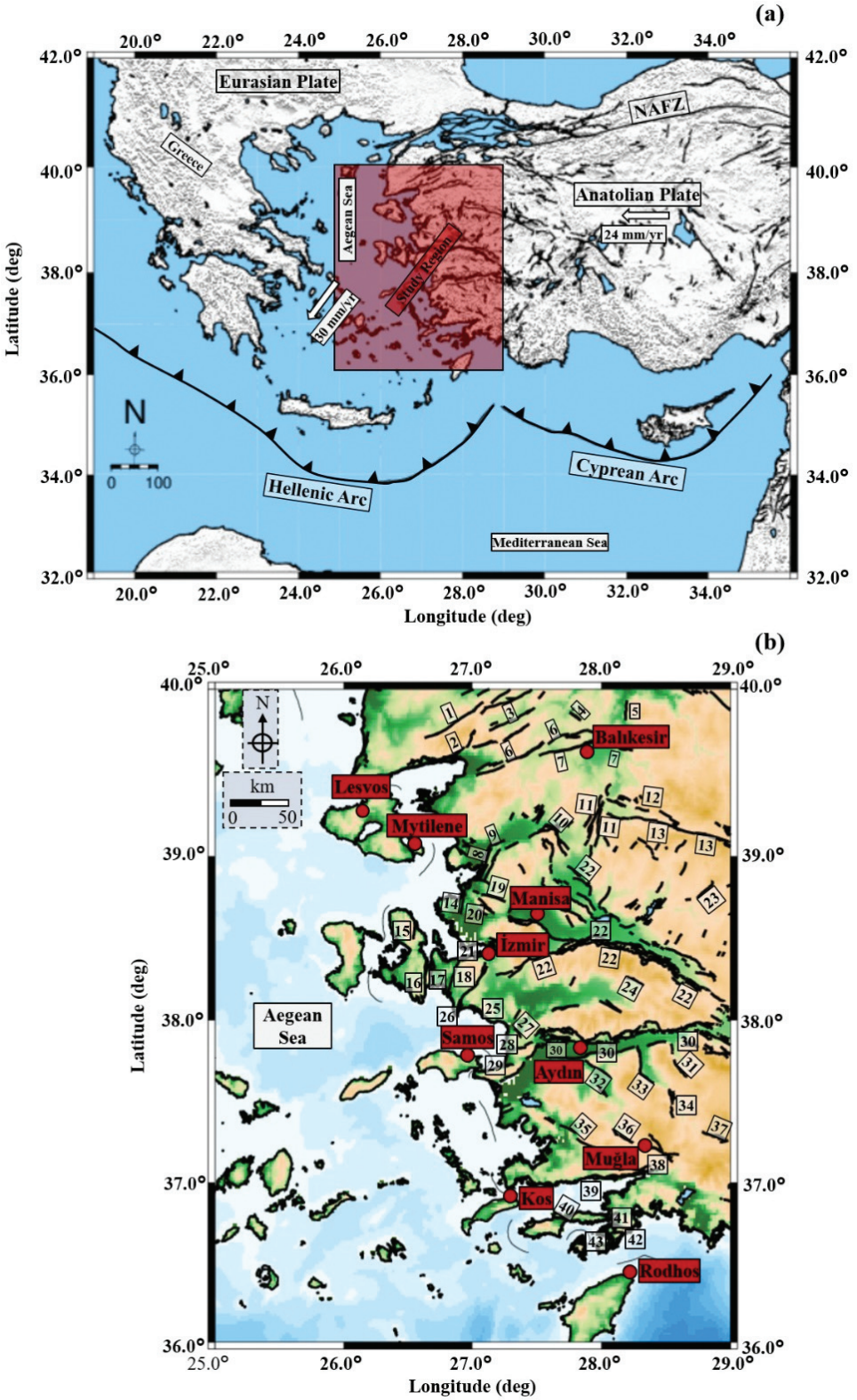

Fig. 1 (a) Major tectonic elements of the Eastern Mediterranean region. Black lines indicate the locations of active faults taken from Li *et al*. (2003), Emre *et al*. (2018), and Utkucu *et al*. (2021). The red rectangle area depicts the study region. Plate velocities are depicted by white arrows (modified from Reilinger et *al*. (2006)). (b) Local tectonic units of the study region (modified from Emre *et al*. (2018)). Claret red circles represent provinces. Faults No: Evciler F: 1, Edremit FZ: 2, Pazarköy F: 3, Samlı F: 4, Susurluk F: 5, Havra-Balyan FZ: 6, Balıkesir F: 7, Zeytindağ FZ: 8, Bergama F: 9, Soma-Kırkağaç FZ: 10, Gelenbe FZ: 11, Düvertepe FZ: 12, Simav FZ: 13, Yenifoça F: 14, Mordoğan F: 15, Gülbahçe FZ: 16, Yağcılar F: 17, Seferhisar F: 18, Güzelhisar F: 19, Menemen FZ: 20, İzmir F: 21, Gediz GS: 22, Selendi F: 23, Kiraz F: 24, Gümüldür F: 25, Tuzla F: 26, Efes F: 27, Kuşadası F: 28, Davutlar F: 29, Büyük Menderes GS: 30, Karacasu F: 31, Çine F: 32, Bozdoğan F: 33, Göktepe F: 34, Milas F: 35, Yatağan F: 36, Beyağaç F: 37, Muğla F: 38, Gökova FZ: 39, Datça F: 40, Selimiye F: 41, Bozburun F: 42, Taşlıca F: 43. *FZ*: Fault Zone, *F*: Fault, and *GS*: Graben System

ger *et al*. 2006; Le Pichon, Kreemer 2010; Taymaz *et al*. 2022).

EARTHQUAKE DATABASE

For the region-time-magnitude analyses of seismotectonic variables, a homogeneous earthquake database according to Mw was compiled by Tan (2021) for the time interval from 1905 to 2019. Tan (2021) proposed a homogeneous catalogue, and the equivalence Mw was the most suitable magnitude type for the earthquake hazard analysis. There were 377.429 events in this catalogue for Türkiye and its vicinity between 1905 and 2019. In addition to this earthquake database, the events with local magnitude, M_L, between 2019 and 2024 were compiled from the Kandilli Observatory and Earthquake Research Institute (KOERI). There were 153.990 earthquakes around Türkiye at that time. To obtain a homogeneous database according to Mw between 2019 and 2024, the empirical relationship from Tan (2021) for Mw–M_L conversion ($Mw = 1.017 * M_L - 0.012$) was considered. 531.419 earthquakes were obtained for Türkiye and its surroundings between 1905 and 2024. After this step, the earthquakes were selected for the study area between 36.0°N – 40.0°N and 25.0°E – 29.0°E. Thus, 189.715 earthquakes with $1.0 \leq Mw \leq 7.8$ between 4 April 1911 and 30 June 2024, about 113.24 years, were obtained. The epicentre locations of all events and the large main shocks with $Mw \geq 6.0$ are plotted in Fig. 2a.

On the other hand, 41 earthquakes with $Mw \geq 5.0$ that occurred in the WAR between 2014 and 2024 were used to investigate the Coulomb stress variation. The focal parameters of earthquakes (dip, strike, rake, etc.) were taken from the Disaster and Emergency Management Authority (AFAD) and United States Geological Survey (USGS) and listed in Table 1. Also, Fig. 2b displays the focal mechanisms and epicentre locations, exhibiting normal fault characteristics. Thus, the stress variations were analyzed according to the normal fault mechanism.

METHODS

Gutenberg-Richter (G-R) relation, magnitude completeness, earthquake probability and return period

The magnitude-frequency distribution of earthquake occurrences can be given with an empirical relationship suggested by Gutenberg, Richter (1944). This scaling is one of the most frequently used forms in earthquake statistics and can be given as follows:

$$\log_{10} N(M) - a - bM \qquad (1)$$

In this formula, $N(M)$ is the cumulative number of earthquakes in a specific time interval with magnitudes $\geq M$. Significant changes can be observed in a- and b-values and they are accepted as positive constants. Although the a-value is related to the earthquake activity rate, the b-value is calculated from the slope of the frequency-magnitude relation. For different seismic regions, some factors such as the length

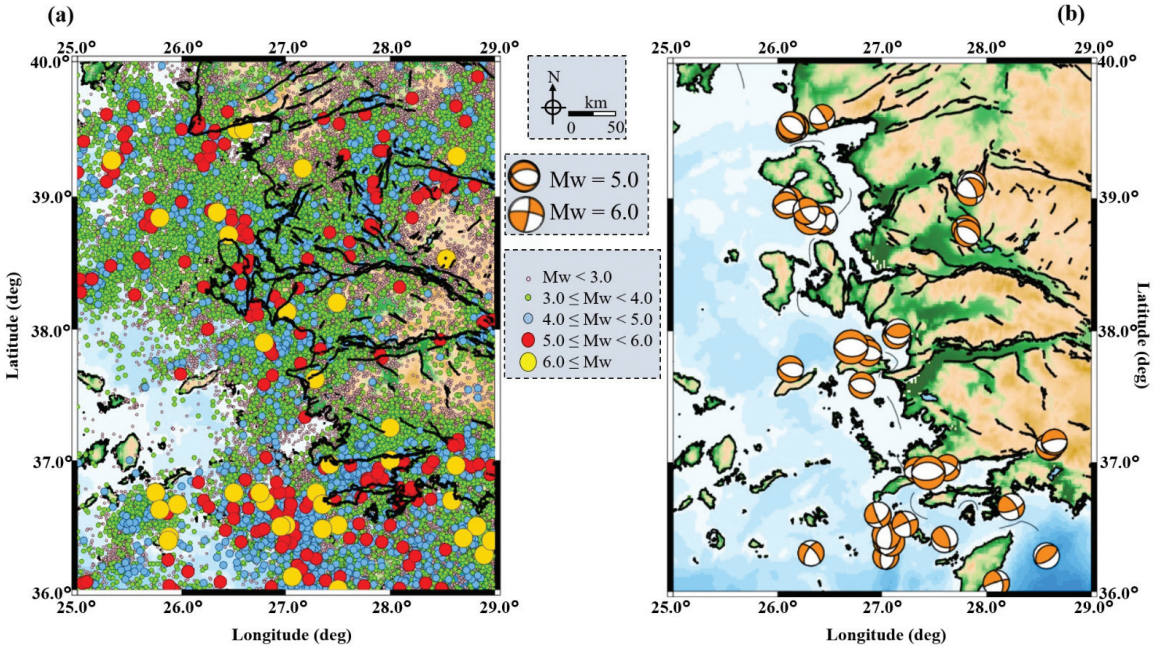

Fig. 2 (a) Epicentre locations of 189.715 earthquakes with $Mw \geq 1.0$ from 1911 to 2024 for the study region. The seismicity catalogue is taken from the KOERI website (https://udim.koeri.boun.edu.tr/). Magnitude levels of the events are plotted with different symbols. (b) Orange beach balls represent the earthquake fault mechanism solutions ($Mw \geq 5.0$). The parameters of the focal mechanism solution are given in Table 1

Table 1 Source parameters of earthquakes taken from the AFAD (https://tdvms.afad.gov.tr/) and USGS (https://www.usgs.gov/) to calculate Coulomb stress changes

No	Date	Longitude (°E)	Latitude (°N)	Depth (km)	Magnitude (Mw)	Strike (°)	Dip (°)	Rake (°)	Fault Type	Source
1	2024-01-27T05:19:19	27.130	37.966	8.51	5.1	109	48	-84		AFAD
2	2023-04-26T20:00:35	26.320	36.297	54.16	5.0	316	65	-147		AFAD
3	2022-08-31T10:10:10	26.807	37.588	7.03	5.1	276	47	-99		AFAD
4	2022-08-14T00:24:22	27.151	37.995	11.7	5.0	94	52	100		USGS
5	2021-11-30T04:00:42	26.122	37.711	7.0	5.1	113	44	-69		AFAD
6	2021-08-07T01:39:45	27.036	36.272	18.4	5.0	4	35	-96		USGS
7	2021-08-03T12:38:17	27.044	36.390	10.0	5.2	358	42	-112		USGS
8	2021-08-01T04:31:27	27.080	36.384	10.86	5.5	228	47	-73		AFAD
9	2021-06-22T01:14:13	27.042	36.439	9.0	5.5	217	39	-51		USGS
10	2021-04-13T20:28:06	27.220	36.521	8.57	5.1	340	63	-172		AFAD
11	2021-02-01T05:46:53	26.118	38.985	20.69	5.1	153	49	-100		AFAD
12	2021-02-01T08:35:17	26.078	38.948	17.62	5.1	108	33	-58		AFAD
13	2020-10-31T05:31:30	26.830	37.870	7.33	5.0	271	52	-98		AFAD
14	2020-10-30T15:14:56	26.869	37.833	7.73	5.1	103	45	-85		AFAD
15	2020-10-30T11:51:23	26.703	37.879	14.9	6.6	95	43	-87		AFAD
16	2020-06-28T17:43:28	28.233	36.656	63.72	5.2	326	62	152		AFAD
17	2020-06-26T07:21:11	27.801	38.767	9.29	5.5	138	62	-80		AFAD
18	2020-02-18T16:09:22	27.845	39.101	14.68	5.2	341	78	-11		AFAD
19	2020-01-28T14:26:15	27.875	39.106	10.0	5.0	111	68	-103		USGS
20	2020-01-22T19:22:16	27.844	39.048	10.35	5.4	94	53	-141		AFAD
21	2019-10-03T07:44:56	28.572	36.277	17.8	5.1	226	31	81		USGS
22	2019-02-20T18:23:28	26.426	39.601	5.8	5.0	329	78	-40		AFAD
23	2019-01-24T17:30:54	28.093	36.065	47.7	5.1	348	50	-171		USGS
24	2017-11-24T21:49:14	28.604	37.114	24.46	5.1	104	41	-87		AFAD
25	2017-11-22T20:22:51	28.592	37.120	24.75	5.0	110	43	-89		AFAD
26	2017-08-08T07:42:21	27.623	36.957	11.03	5.1	53	48	-138		AFAD
27	2017-07-21T17:09:48	27.332	36.941	37.5	5.0	61	40	-107		AFAD
28	2017-07-20T22:31:09	27.443	36.919	19.44	6.5	275	38	-80		AFAD
29	2017-06-22T02:48:52	26.453	38.821	13.5	5.0	242	41	-151		AFAD
30	2017-06-17T19:50:04	26.436	38.838	10.25	5.3	235	78	-169		AFAD
31	2017-06-12T12:28:37	26.313	38.848	7.0	6.2	127	45	-54		AFAD
32	2017-05-27T15:53:23	27.815	38.735	11.03	5.1	298	55	-100		AFAD
33	2017-04-13T16:22:16	28.647	37.153	11.33	5.0	260	72	-93		AFAD
34	2017-02-12T13:48:16	26.170	39.533	7.0	5.3	107	49	-115		AFAD
35	2017-02-10T08:55:25	26.175	39.523	7.79	5.0	144	44	-83		AFAD

No	Date	Longitude (°E)	Latitude (°N)	Depth (km)	Magnitude (Mw)	Strike (°)	Dip (°)	Rake (°)	Fault Type	Source
36	2017-02-07T02:24:03	26.116	39.514	11.92	5.2	132	29	-75		AFAD
37	2017-02-06T10:58:02	26.137	39.527	9.83	5.3	113	50	-93		AFAD
38	2017-02-06T03:51:40	26.131	39.542	8.86	5.3	129	54	-80		AFAD
39	2016-12-20T06:03:45	26.959	36.594	118.3	5.1	59	46	-12		AFAD
40	2016-09-27T20:57:09	27.596	36.405	50.63	5.2	109	40	46		AFAD
41	2014-12-06T01:45:06	26.274	38.904	22.48	5.1	254	67	-148		AFAD

of the study area, time interval of the earthquake catalogue, as well as the number of earthquakes are effective on the changes of the *a*-value. However, many factors such as the anisotropic structure, tectonic features, stress distributions, geological complexity, thermal gradient, fault length, material properties, crack density, seismic attenuation, seismic wave velocity changes, slip distribution, or strain circumstances lead to changes in the *b*-value (Mogi 1962; Schorlemmer *et al*. 2005; Öztürk *et al*. 2008; Scholz 2015). Also, relative distributions of small and great events affect *b*-value variations. Although the *b*-value varies from 0.3 to 2.0 on the global scale (Utsu 1971), it is proposed that the average *b*-value equals 1.0 (Frohlich, Davis 1993). Thus, the *b*-value is accepted as a crucial variable for the earthquake statistic in the seismically and tectonically active regions.

In many studies associated with seismicity rate changes and especially in the calculation of the *b*-value, it is very important to use the maximum number of earthquakes for reliable and high-quality results. In this context, the estimation of magnitude completeness, *Mc*-value, which is the minimum magnitude of complete recording, must be the first step before these types of analyses. The *Mc*-value is determined from the magnitude-frequency distribution of earthquakes and this completeness level includes 90% of the earthquakes (Wiemer, Wyss 2000). The *Mc*-value may be larger in the early time of the catalogue since small events may not be located and they fall within the coda of greater earthquakes (Wiemer, Katsumata 1999). Since the *Mc*-value changes regionally, depending on the earthquake activity of the region under investigation and the detectability of the network, the variations in the *Mc*-value in time can affect the statistical results. For this reason, temporal changes in the *Mc*-value must be carried out carefully and a moving time window approach with the maximum likelihood approach may be used (Wiemer, Wyss 2000).

The occurrence probabilities of different earthquake magnitudes (*M*) for certain time intervals (*Tr*) may be determined from the following equation (Tabban, Gençoğlu 1975):

$$P(M) = 1 - e^{-N(M)*Tr} \quad (2)$$

In this equation, $P(M)$ is the occurrence probability that at least one earthquake can occur in *Tr* years. $N(M)$ is calculated from the G-R relation (Eq. 1), and *Tr* can be given as different periods such as 10, 20, 30, …, 100 years, etc. Equation 2 is a result of the Poisson distribution. The return period of an earthquake with a certain magnitude level may be calculated from the following formula (Tabban, Gençoğlu 1975):

$$Q(M) = 1 / N(M) \quad (3)$$

In this equation, $Q(M)$ is the return period of an earthquake and it is accepted as the expected time interval for an earthquake with a magnitude ≥ *M*.

Coulomb stress changes

Earthquakes called natural phenomena are considered the result of stress releasing when shear stresses across earthquake fault planes exceed fault strength (Yang *et al*. 2024). Because of this, Coulomb stress changes are crucial to analyzing the earthquake-induced stress change (Peikert *et al*. 2023). Therefore, Coulomb stress analysis is the well-known approach to researching the stress changes under which a failure occurs in the source fault. The Coulomb failure stress ($\Delta\sigma_{cfs}$) change depends upon the receiver fault as follows:

$$(\Delta\sigma_{cfs}) = \Delta\tau_s + \mu'\Delta\sigma_{n'} \quad (4)$$

Here, $\Delta\tau_s$ symbolizes the shear stress change associated with the positive direction of receiver fault slip, $\Delta\sigma_{n'}$ is the normal stress change along the fault plane, and μ' is the effective friction coefficient on the fault (King *et al*. 1994; Lin, Stein 2004; Toda *et al*. 2011). μ' means the effects of pore-pressure changes and varies from 0 to 1. For this study, we consider 0.4 in an elastic half-space (Toda *et al*. 2005; Wan, Shen 2010). We assume the dimensionless Poisson's ratio (*v*) is 0.25 and Young modulus (*E*) is chosen as 8×10^5 bars. The Coulomb stress observation between -0.1 and 0.1 (bar) is satisfactory to forecast the following earthquake hazards (Yadav *et al*. 2012). The increase in the Coulomb stress changes indicates the loading stress, pushing the fault toward brittle failure, while the decreased changes may correspond to the

unloading stress, inhibiting the rupture of the earthquake (Stein *et al*. 1994; Liao *et al*. 2022; Peikert *et al*. 2023).

RESULTS

A comprehensive statistical and seismotectonic appraisal of the current and future earthquake hazard for the WAR, which is a very seismically active region of Türkiye, was accomplished by analysis and combinations of the results of parameters such as (i) the *b*-value of G-R relation and time-magnitude analyses of the earthquakes, (ii) Coulomb stress changes, and (iii) the occurrence probabilities and return periods of strong earthquakes. To make a satisfactory assessment of the earthquake occurrences, regional and depth-dependence variations of these parameters were mapped for mid-2024.

The magnitude histogram of the earthquakes between 1911 and 2024 is given in Fig. 3a. The earthquake catalogue includes 189.715 earthquakes with Mw ≥ 1.0. As seen in Fig. 3a, there exists a clear change between 1.0 and 3.0, and a maximum can be seen in Mw = 2.5. There are 168.398 events with 3.0 > Mw, 19.173 events with 4.0 > Mw ≥ 3.0, 1888 events with 5.0 > Mw ≥ 4.0, 218 events with 6.0 > Mw ≥ 5.0, and 38 events with 6.0 ≤ Mw. Thus, for a detailed time-magnitude analysis and completeness value, a magnitude histogram is considered. For reliable statistical results, it is very important to use the maximum number of events. Hence, the determination of the *Mc*-value is considered the first step for the region-time-magnitude analyses of the seismicity since the *Mc*-value shows temporal changes. Temporal variations in the *Mc*-value can be calculated with a moving time window approach (Woessner, Wiemer 2005). In this work, the temporal variation of the *Mc*-value was determined with its standard deviation for every 5000 events per window. The temporal change in the *Mc*-value is plotted in Fig. 3b by using the whole catalogue. The *Mc*-value changes between 2.8 and 3.2 until 1996. Then, it varies around 2.8 from 1996 to 2008, and it changes between 2.0 and 2.8 from 2008 to 2014. However, it is smaller than 2.0 after 2014. This change in the *Mc*-value is not stable in time, and a clear fluctuation exists between 2.0 and 3.0 from 1991 to 2014 and between 1.5 and 2.0 from 2014 to 2024. Thus, the *Mc*-value was accepted as 2.5, and this value follows the literature studies such as Öztürk (2015) and Bayrak *et al*. (2017).

The cumulative number of earthquakes during the period of the catalogue is given in Fig 4a. The original catalogue includes 189.715 events with Mw ≥ 1.0, whereas the complete catalogue contains 60.847 earthquakes with Mw ≥ 2.5. As seen in Fig. 4a, any significant increases did not exist in the earthquake numbers from 1911 to 1980, and there were very few earthquakes between 1980 and 2000. However, a rapid increase in seismicity can be seen after 2000, especially after 2010. Also, the cumulative number of earthquakes for the complete catalogue with Mw ≥ 2.5 has a smooth slope compared to the original database. It is well known that this process is necessary to ensure the completeness in the catalogue, and the analysis of the magnitude of completeness must be considered a significant step for a qualified assessment of the seismic potential and hazard. Thus, the completeness process (excluding the events with Mw < 2.6 from the catalogue) provided a more uniform database for the region-time-magnitude evaluation. Figure 4b shows the magnitude-frequency distribution and the *b*-value of the G-R relation. *a*- and *b*-values were obtained as 6.98 and 0.91 ± 0.07, respectively, with the maximum likelihood technique by using the original database with *Mc* = 2.5. As mentioned above, on the global scale, the *b*-value changes from 0.3 to 2.0, and tectonic earthquakes are characterized by the *b*-value between 0.5 and 1.5, despite the average *b*-value being suggested as ~1.0. Thus, the magnitude-frequency distribution of the earthquakes for the study region is well represented by the G-R relation with the *b*-value typically ~ 1.0, and the

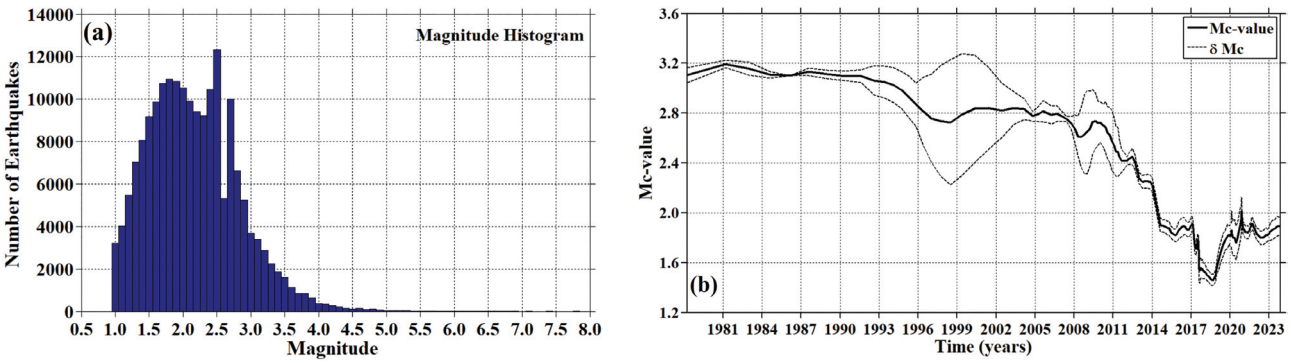

Fig 3 (a) Magnitude histogram of the earthquake occurrences between 1911 and 2024. (b) Changes of magnitude completeness, *Mc*-value, in time. The standard deviation, δ*Mc*, was also drawn. The *Mc*-value was determined with the moving window approach and 5000 earthquakes in each window

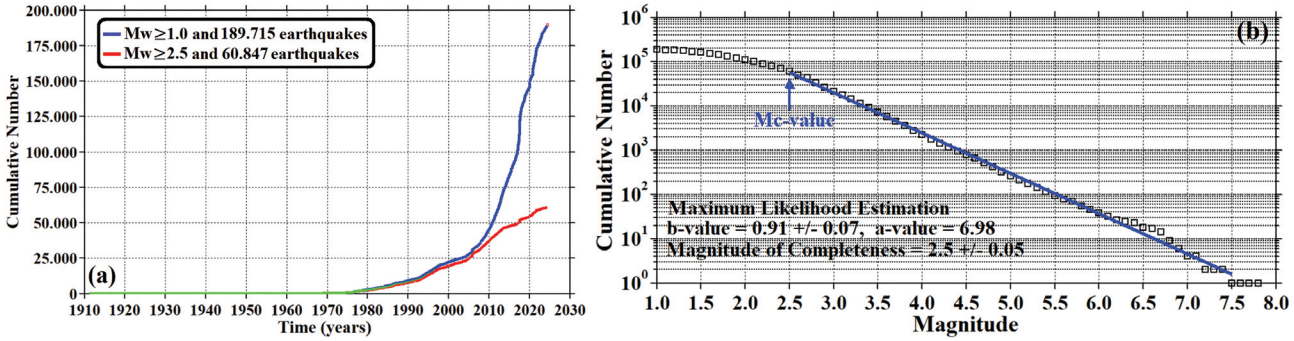

Fig. 4 (a) Cumulative number of earthquakes from 4 April 1911 to 30 June 2024 for the whole catalogue with Mw ≥ 1.0 (blue line) and the complete catalogue with Mw ≥ 2.5 (red line). (b) Magnitude-frequency distribution of the earthquakes and the *b*-value of G-R relation. *a*- and *Mc*-values are also given on the figure

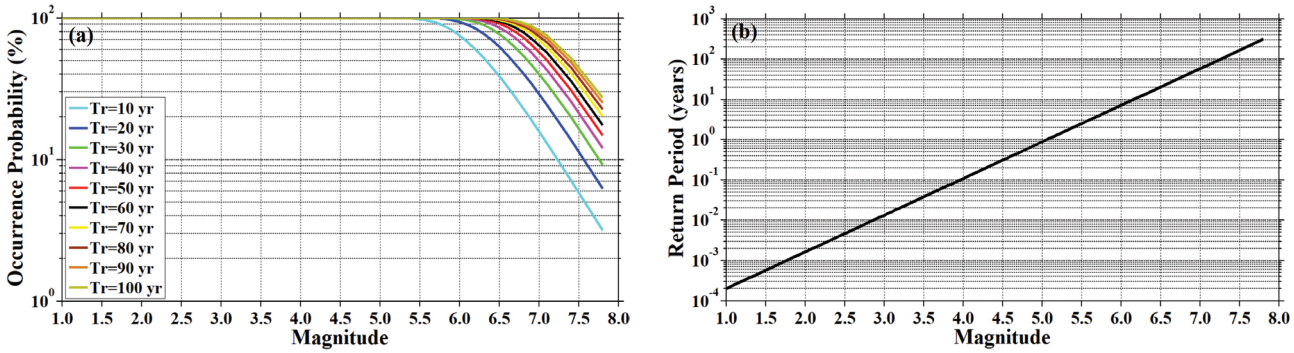

Fig. 5 (a) Occurrence probabilities of the earthquakes for all magnitude values in the catalogue and specific values of *Tr* (years) = 10, 20, 30, 40, 50, 60, 70, 80, 80, 90, 100 for the possibilities. (b) Return periods of the earthquakes for all magnitude values in the catalogue

b-value of 0.91 can be interpreted as a relatively low value.

A significant application for the statistical appraisal of earthquake hazard is well known as the estimation of occurrence probabilities and return periods of strong/large earthquakes. For this purpose, these variables for whole magnitude levels in the catalogue were calculated and drawn in Fig. 5. As seen from Fig. 5a, occurrence probabilities between 90% and 100% were estimated for the earthquakes of 1.0 ≤ Mw < 5.5 for all the certain years (*Tr* = 10, 20, …., 100). In addition, the occurrence probabilities of an earthquake with Mw = 6.0 change between 70% and 100%, whereas the values for different *Tr* values are relatively larger than 35% for the earthquakes with Mw = 6.5 (Fig. 5a). According to the results (also seen in Fig. 5a), the occurrence probabilities of Mw = 7.0 in *Tr* = 10, 20 and 50 years were estimated as ~ 16%, ~ 28%, and ~ 58%, respectively. The probabilities of Mw = 7.5 in *Tr* = 10, 20, and 50 years were calculated as ~6%, ~12% and ~26%, respectively. Also, the occurrence probabilities of an earthquake with Mw = 7.8 in *Tr* = 10, 20, and 50 years were found as ~ 3%, ~ 6%, and ~15%, respectively. In addition to these certain values, the occurrences probabilities of all magnitude levels for all *Tr* years were plotted in Fig. 5a. The return periods of the earthquakes with all magnitudes were plotted in Fig. 5b. As shown in Fig. 5b, relatively small return periods (< 1.0 years) were estimated for magnitudes between 1.0 and 5.0. However, for magnitudes from 5.0 to 6.5, return periods were estimated between 1 and 20 years. Return periods between 20 and 50 years can be expected for earthquake magnitudes from 6.5 to 7.0, whereas return periods greater than 50 years can be seen for magnitudes larger than 7.0. As seen in Fig. 5b, the return periods of earthquakes with Mw = 7.0, 7.5, and 7.8 are calculated as ~55, ~160, and ~311 years, respectively. The return periods of all earthquake magnitudes can also be easily found in Fig. 5b. The estimated values for probabilities and return periods indicate that earthquake occurrences between 5.0 and 6.5 in the intermediate/long terms are more likely than those of other magnitude levels.

To analyze the changes in the *b*-value in different depths, the regional behaviours of the *b*-value for every 10 km depth intervals were evaluated and are plotted in Fig. 6. To image the *b*-value, a moving window method with the maximum curvature approach defined in Woessner, Wiemer (2005) was used. For these analyses, different sample sizes depending on a different number of earthquakes in each depth were used and a spatial grid of 0.1° × 0.1° in longitude and latitude was considered for all depths. Regional

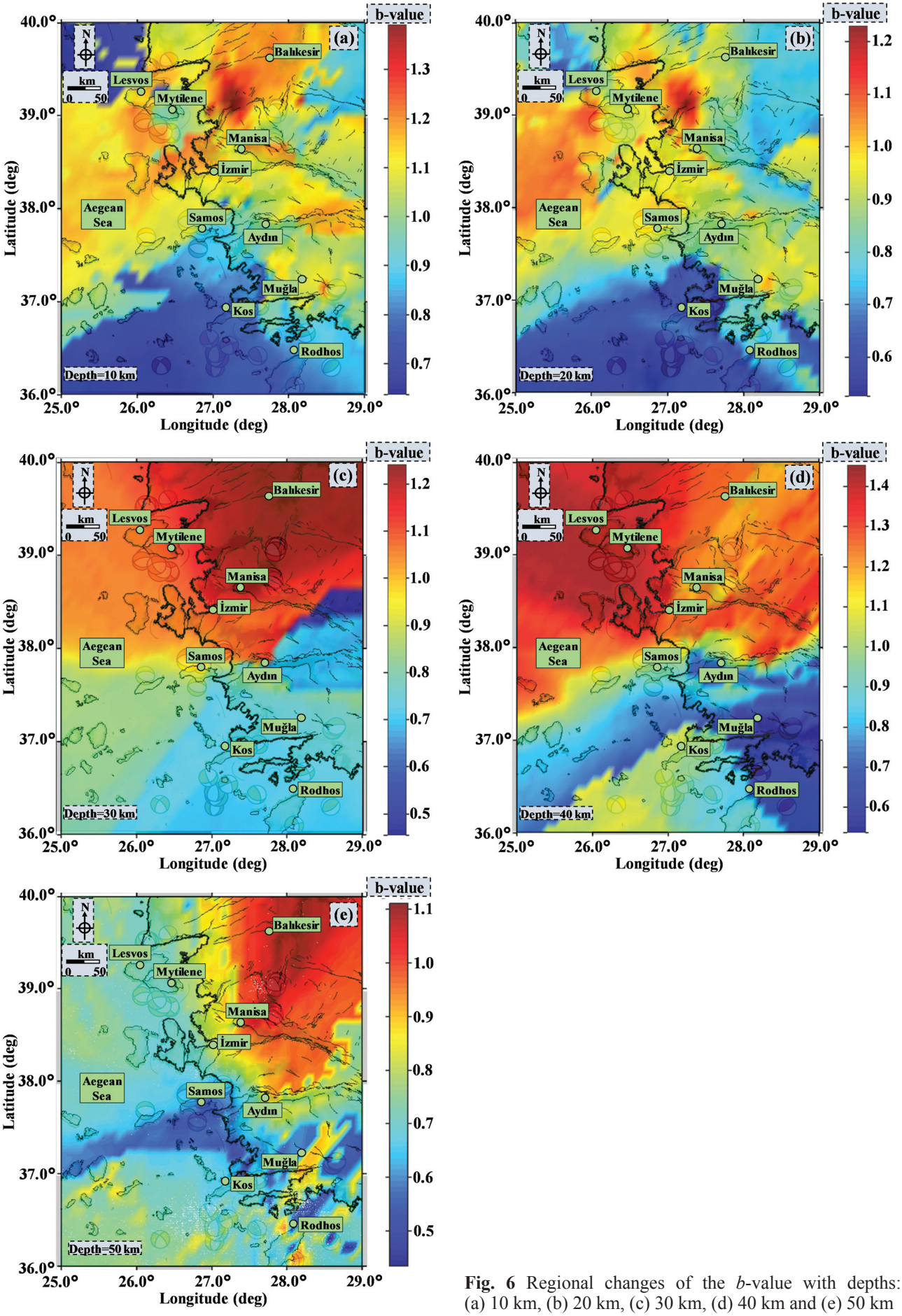

Fig. 6 Regional changes of the *b*-value with depths: (a) 10 km, (b) 20 km, (c) 30 km, (d) 40 km and (e) 50 km

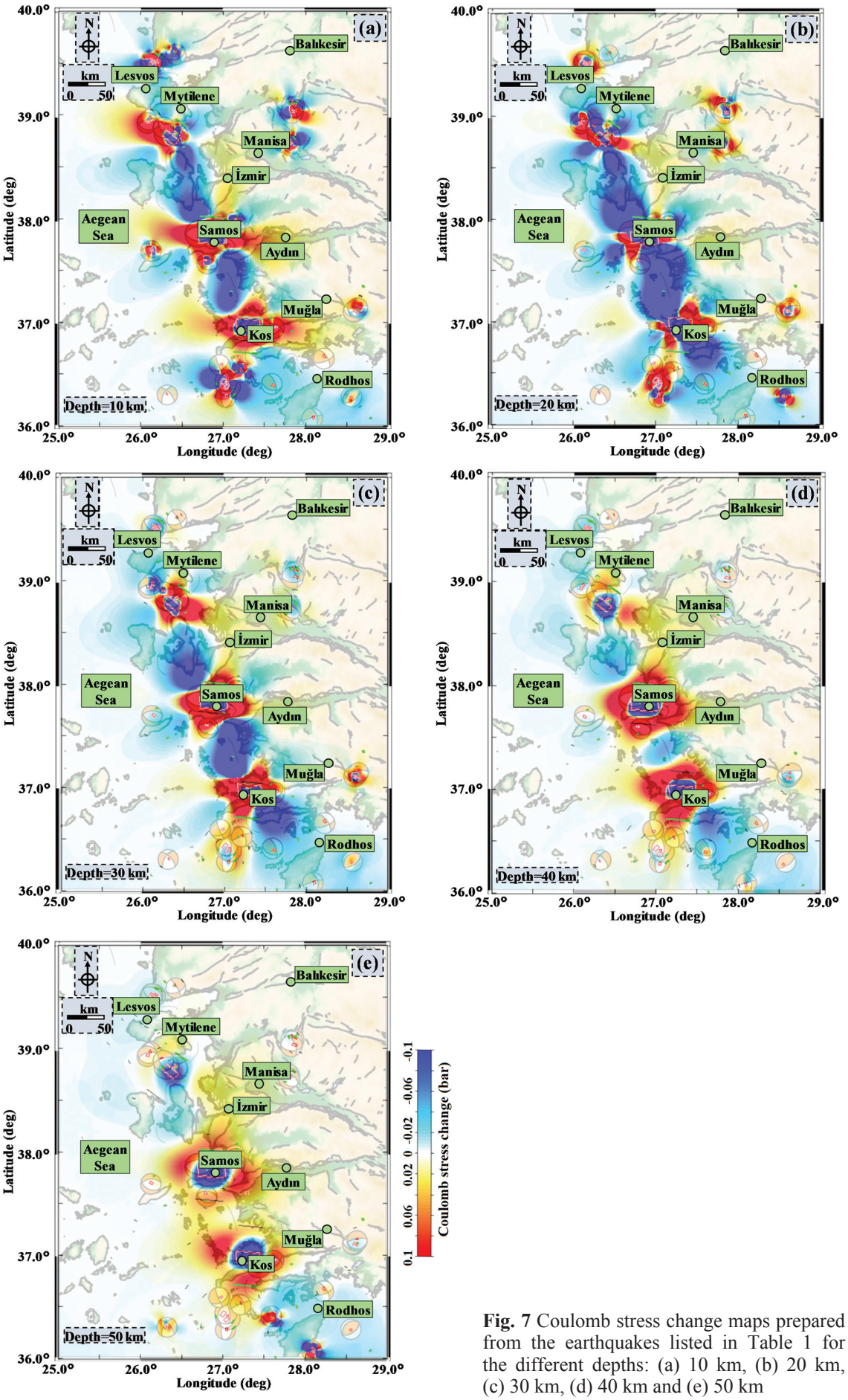

Fig. 7 Coulomb stress change maps prepared from the earthquakes listed in Table 1 for the different depths: (a) 10 km, (b) 20 km, (c) 30 km, (d) 40 km and (e) 50 km

changes in the *b*-value for different depths have values between 0.43 and 1.45. As imaged in Fig. 6a, for the depth of 10 km, there exist strong decreases (< 0.9) including Rodhos, Kos, Aydın, and Samos regions, the northwest part of the study region, and the eastern part of Balıkesir (including Gelenbe FZ, Düvertepe FZ, Simav FZ, Yenifoça F). The rest parts of the study region including İzmir, Manisa, and Muğla have large *b*-values (> 1.1). Similar changes were roughly observed in the same areas for the depth of 20 km (Fig. 6b). However, there exist several regions with small *b*-values including Pazarköy F, Gediz GS, and Selendi F. For the depth of 30 km (Fig. 6c), the *b*-value reflects a clear increase (> 1.0) for the north, northeast, and northwest parts, whereas a remarkable decrease (< 0.8) can be seen in the east, south, and southeast parts of the study region. Very similar variations were obtained for the depth of 40 km (Fig. 6d), and small (< 0.8) and large (1.1 <) *b*-values can be seen in the same parts with a depth of 30 km. For the depth of 50 km (Fig. 6e), the smallest *b*-values (< 0.7) were shown in and around İzmir, Samos, Muğla Kos, Rodhos, whereas great *b*-values (> 1.0) were imaged in the northeast part of the study area.

Figure 7 shows Coulomb stress change results in the depth range of 10–50 km. The positive anomalies (in red colours) that appeared from Coulomb stress maps represent the high-stress regions, while negative anomalies (in blue colours) that appeared from Coulomb stress maps correspond to the low-stress regions. In the maps, all depth levels are examined for the positive stress values (> 0.0 in a bar) under the Samos and Kos Islands. In this region, there are Samos, Kuşadası, and Datça faults. These faults show the normal fault characters in the E–W direction with N–S extension (Emre *et al*. 2018; Över *et al*. 2021). On the contrary, there is a decrease in stress to the north and south of Samos and Kos Islands. These negative stress lobes can be seen especially at depth levels of 10–30 km. Also, we focus on the south of Lesvos Island and west of Manisa province, lined with the positive stress changes in the NW–SE direction at the crustal depths, while the negative stress lobe can be seen at the uppermost lithospheric depths. Several important fault mechanisms have been observed between Lesvos and Manisa provinces. Lesvos, Yenifoça, Güzelhisar, and Menemen faults. In 2017, the Lesvos fault produced an important earthquake (Table 1, event no 31) that occurred in a shallow depth (7 km). These current earthquakes and stress distribution may be related to the movement of the Hellenic Trench associated with African slab roll-back (Över *et al*. 2021). On the other hand, positive stress variations can be observed in Aydın and Muğla provinces, especially at shallow depths. This region has the tectonic structures of normal fault mechanism called Büyük Menderes Graben System, Gökova fault zone, and Muğla fault in particular.

DISCUSSION

Many studies including different statistical, seismic, and tectonic parameters of earthquake occurrences in the WAR can be found in the literature. In this scope, in recent years, many authors provided a comprehensive appraisal of seismotectonic, structural, geological, or geodetic variables based on the combination of different geophysical data (Bayrak *et al*. 2017; Kiratzi *et al*. 2020; Sboras *et al*. 2020; Bulut *et al*. 2021; Diercks *et al*. 2023; Çırmık *et al*. 2024). These analyses revealed that the WAR is a high-potential seismic hazard related to the occurrences of major earthquakes in the short/medium/long term. Although there can be many studies with different parameters for the WAR, these types of statistical and seismotectonic appraisal of the earthquake potential are relatively rare. Thus, a comprehensive regional and temporal analysis is aimed at the current earthquake potential and forecasting in the intermediate term.

Bayrak *et al*. (2017) made a spatiotemporal evaluation of earthquake activity for Western Anatolia by considering the *b*-value and *Dc*-value. They observed the smallest *b*-values and the largest *Dc*-values in the Aegean Arc and related to the Eskişehir fault. Also, they proposed that the regional mapping of the *b*-value supplies useful information about the stress variations of the region. Thus, they stated that smaller *b*-values are related to the possible locations of future earthquakes. Kiratzi *et al*. (2020) studied the characteristics of the 2020 Samos earthquake by using a spatial and temporal distribution of aftershock activity and stress transfer. Their slip model showed that the aftershock sequence ruptured the upper crust in the depth range between 3 and 15 km. They stated that Samos Island and İzmir province have a rich seismic history and complex geotectonic structures, hence earthquake hazard factors must be taken into consideration in the long-term development planning of the eastern Aegean region. Sboras *et al*. (2020) studied fault modelling, seismic sequence, and stress changes for the 2017 (Mw = 6.6) Gökova Gulf earthquake by using seismological and geological variables. According to their results, the N–S directional crustal stretching and regional-temporal evolution show long quiescence. Also, observations for the post-sequence stress change suggested that this region is fully loaded with the positive stress. Bodrum and Datça peninsulas are related to the decreased stress regions, referring to a possible delay of future seismic activity. Bulut *et al*. (2021) made a study on the rupture geometry, size, and slip distribution of the 2020 Samos-Kuşadası earthquake considering seismographs, SAR analysis,

and GPS measurements. They also tried to reveal the earthquake hazard in the Aegean Sea by investigating Coulomb stress changes following strong earthquakes. According to their results, the main shock of the Samos earthquake increased Coulomb stress on some fault segments near Kuşadası and Söke provinces. They suggested that increased Coulomb stress on the segments of the south of İzmir gives a warning for the current seismic hazard in this highly inhabited region of the WAR. Utkucu *et al*. (2021) investigated the 2017 Karaburun–Lesvos earthquake (Mw = 6.2) and its aftershocks that occurred on the Lesvos fault. This region is located in the west of Manisa province. The authors expressed that the positive stress orientation of the main shock is in good agreement with the aftershocks on the NW–SE striking. Diercks *et al*. (2023) supplied a model by using Coulomb stress change to evaluate the historical earthquake occurrence and constrain the possible source faults. This approach was used to model the coseismic and interseismic stress variation over 400 years for the Büyük-Menderes Graben region. By modelling multiple possible historical earthquake scenarios and subsequent evaluation of earthquake occurrences, they suggested that the current stress state is related to earthquake hazard in tectonically active regions. Çırmık *et al*. (2024) made the coseismic and postseismic displacement assessments of the 30 October 2020 (Mw = 6.9) Samos earthquake. They used GNSS data before, during, and after the main shock to examine the earthquake effects. Also, they analyzed the horizontal displacement by using the Coulomb failure criteria as well as peak ground displacements. Their displacement analyses show that high-amplitude energy was released from Ayvalık province in the north to Datça province in the south after the main shock, and this earthquake generated continuous deformation in the earthquake region. These results showed that a significant earthquake hazard may be in the intermediate/long term in the WAR. Thus, spatial and temporal analyses of geophysical and geodetic parameters and a combined evaluation of stress changes because of the coseismic and postseismic displacements may provide a more detailed interpretation to make a reliable earthquake hazard and forecasting for the study region.

As discussed above, some anomaly areas show small *b*-values and great Coulomb stress changes in several parts of the WAR such as Mytilene, Samos, Kos, Muğla, and Rodhos, around Gediz graben. The smallest *b*-values are considered to be evidence for the great stress release, and the smallest *b*-values are commented as a sign of large strain due to the active tectonics of the study area. These small *b*-values may also be a sign of the increasing stress with time and are released by earthquakes that are less frequent but great in magnitude (Öncel, Wilson 2007). Therefore, small *b*-values and large stress areas may indicate the locations of the next possible earthquakes. For this reason, a combined appraisal of these types of seismotectonic variables may supply more reliable information for the current earthquake hazard and successful forecasting in the WAR. As stated above, this area was struck with strong/large earthquakes in the past and many moderate/great events have occurred in the WAR in recent years. Therefore, special attention should be given to all anomaly areas of estimated parameters. Thus, these types of hazard and forecasting studies in this area would be essential, and these types of assessments must rely on the monitoring and/or analyzing of different geophysical tools.

CONCLUSIONS

A combined assessment of the seismotectonic tools such as the *b*-value, occurrence probabilities, return periods, and Coulomb stress changes are performed for a satisfactory earthquake hazard and forecasting of the next earthquake location in the West Anatolian Region of Türkiye. This region has been struck with moderate and destructive earthquakes in recent years.

Based on an analysis of the results of the parameters we observe that the areas covering the west and southwest part of the study region, Samos Island, Kos Island, south of Lesvos Island, and the western part of Büyük Menderes and Gediz Graben Systems have corresponded with a low *b*-value and increased stress. These regions are relatable with the highest seismic potential. It is well known that the areas with small *b*-values and positive-stress values are the most likely locations where the next strong earthquakes will be expected to occur. Conversely, Coulomb stress changes performed by local earthquakes with mostly normal fault character show a stress decrease particularly at shallow/crustal depths (10 km to 30 km) in the Aegean coasts. Besides, analyses of occurrence probabilities and return periods show that the West Anatolian Region has an intermediate or long-term earthquake hazard after mid-2024 with the possible occurrence of great earthquakes with Mw $\geq$ 6.0. Finally, our results may imply that these correlations supply a better understanding of statistical and seismic properties in the region. In the scope of these findings, we strongly suggest that more encouraging research and time of the future possible earthquakes must cover a combination of multiple parameter analyses.

ACKNOWLEDGMENTS

Some images are obtained from ZMAP and GMT (Wiemer, 2001; Wessel *et al*. 2019). The maps of Coulomb stress changes are created by using the Coulomb 3.3 package (Toda *et al*. 2011). Tectonic units

are digitized in the Geoscience map viewer (Emre *et al*. 2018). We are grateful to KOERI, AFAD, and USGS for providing us with the earthquake database via the Internet. The authors would like to thank anonymous reviewers for their useful and constructive suggestions which have improved this paper and also the Editor-in-Chief for his editorial suggestions.

REFERENCES

Akar, F. 2021. Analysis of the b-Values Before the July 21th, 2017 Mw 6.6 Bodrum-Kos, Turkey, Earthquake. *Erzincan University, Journal of Science and Technology14* (*2*), 382–394. https://doi.org/10.18185/erzifbed.871960

Aktuğ, B., Nocquet, J.M., Cingöz, A., Parsons, A., Erkan, Y., England, P., Lenk, O., Gürdal, M.A., Kilicoglu, A., Akdeniz, H., Tekgül, A. 2009. Deformation of western Turkey from a combination of permanent and campaign GPS data: limits to block-like behaviour. *Journal of Geophysical Research 114* (*B10404*), 1–22. https:// doi.org/10.1029/2008jb006000

Bayrak, E., Yılmaz, Ş., Bayrak, Y. 2017. Temporal and spatial variations of Gutenberg-Richter parameter and fractal dimension in Western Anatolia, Turkey. *Journal of Asian Earth Sciences 138*, 1–11. http://dx.doi.org/10.1016/j.jseaes.2017.01.031

Bozkurt, E. 2001. Neotectonics of Turkey – a synthesis. *Geodinamica Acta 14*, 3–30. https://doi.org/10.1016/S0985-3111(01)01066-X

Bulut, F., Doğru, A., Yaltırak, C., Yalvaç, S., Elge, M. 2021. Anatomy of October 30, 2020, Samos (Sisam) – Kuşadası earthquake (MW 6.92) and its influence on Aegean earthquake hazard. *Turkish Journal of Earth Sciences 30*, 425–435. https://doi.org/10.3906/yer-2102-18

Coban, K.H., Sayıl, N. 2019. Evaluation of earthquake recurrences with different distribution models in western Anatolia. *Journal of Seismology 23*, 1405–1422. https://doi.org/10.1007/s10950-019-09876-5

Console, R., Murru, M., Catalli, F., Falcone, G. 2007. Real time forecasts through an earthquake clustering model constrained by the rate-and-state constitutive law: comparison with a purely stochastic ETAS model. *Seismological Research Letters 78*, 49-56. https://doi.org/10.1785/gssrl.78.1.49

Çırmık, A., Pamukçu, A.A., Doğru, F., Cingöz, A., Özdağ, C., Sözbilir, H. 2024. Displacement analysis of the October 30, 2020 (Mw = 6.9), Samos (Aegean Sea) earthquake. *Journal of Geodetic Science 14*, 1–23, https://doi.org/10.1515/jogs-2022-0166

Dewey, J.F., Şengör, A.M.C. 1979. Aegean and surrounding regions-complex multi-plate and continuum tectonics in a convergent zone. *Geological Society of America Bulletin 90* (1), 89–92. https://doi.org/10.1130/0016-7606(1979)90<84:AASRCM>2.0.CO;2

Diercks, M.L., Mildon, Z.K., Boulton, S.J., Hussain, E., Alçiçek, M.C., Yıldırım, C., Aykut, T. 2023. Constraining historical earthquake sequences with Coulomb Stress Models: An example from western Türkiye. *Journal of Geophysical Research: Solid Earth 128*, 1–16. https://doi.org/10.1029/2023JB026627

Emre, Ö., Duman, T.Y., Özalp, S., Şaroğlu, F., Olgun, Ş., Elmacı, H., Çan, T. 2018. Active fault database of Turkey. *Bulletin of Earthquake Engineering 16*, 3229–3275. https://doi.org/10.1007/s10518-016-0041-2

Frohlich, C., Davis, S. 1993. Teleseismic *b*-values: Or, much ado about 1.0. *Journal of Geophysical Research 98* (*B1*), 631–644. https://doi.org/10.1029/92JB01891

Gutenberg, R., Richter, C.F. 1944. Frequency of earthquakes in California. *Bulletin Seismological Society of America 34*, 185–188. https://doi.org/10.1038/156371a0

Holliday, J.R., Chen, C-C., Tiampo, K.F., Rundle, J.B., Turcotte, D.L., Donnellan, A. 2007. A RELM earthquake forecast based on Pattern Informatics. *Seismological Research Letters 78* (*1*), 87–93. https://doi.org/10.1785/gssrl.78.1.87

Kagan, Y.Y., Knopoff, L. 1987. Statistical short-term earthquake prediction. *Science 236* (*4808*), 1563–1567. https://doi.org/10.1126/science.236.4808.1563

King, G.C., Stein, R.S., Lin, J. 1994. Static stress changes and the triggering of earthquakes. *Bulletin Seismological Society of America 84* (*3*), 935–953. https://doi.org/10.1785/BSSA0840030935

Kiratzi, A., Papazachos, C., Özacar, A., Pinar, A., Kkallas, C., Sopaci, E. 2020. Characteristics of the 2020 Samos earthquake (Aegean Sea) using seismic data. *Bulletin of Earthquake Engineering 20*, 7713–7735. https://doi.org/10.1007/s10518-021-01239-1

Le Pichon, X., Kreemer, C. 2010. The miocene-to-present kinematic evolution of the Eastern Mediterranean and Middle East and its implications for dynamics. *Annual Review of Earth and Planetary Sciences 38*, 323–351. https://doi.org/10.1146/annurev-earth-040809-152419

Li, X., Bock, G., Vafidis, A., Kind, R., Harjes, H.-P., Hanka, W., Wylegalla, K., van der Meijde, M., Yuan, X. 2003. Receiver function study of the Hellenic subduction zone: imaging crustal thickness variations and the oceanic Moho of the descending African lithosphere. *Geophysical Journal International 155* (*2*), 733–748. https://doi.org/10.1046/j.1365-246X.2003.02100.x

Liao, B.Y., Huang, H.C., Xie, S. 2022. The source characteristics of the M 6.4, 2016 Meinong Taiwan earthquake from teleseismic data using the hybrid homomorphic Deconvolution method. *Applied Sciences 12* (*494*), 1–13. https://doi.org/10.3390/app12010494

Lin, J., Stein, R.S. 2004. Stress triggering in thrust and subduction earthquakes and stress interaction between the southern San Andreas and nearby thrust and strike-slip faults. *Journal of Geophysical Research: Solid Earth*, *109* (*B2*). https://doi.org/10.1029/2003JB002607

Matsumura, S. 1993. Overestimates of earthquake prediction efficiency in a "postprediction" state. *Journal of Physics of the Earth 41* (*1*), 41–43. https://doi.org/10.4294/jpe1952.41.41

McClusky, S., Balassanian, S., Barka, A., Demir, C., Ergintav, S., Georgiev, I., Gurkan, O., Hamburger, M., Hurst, K., Kahle, H., Kastens, K., Kekelidze, G., King, R., Kotzev, V., Lenk, O., Mahmoud, S., Mishin, A., Nadariya, M., Ouzounis, A., Paradissis, D., Peter, Y., Prilepin, M., Reilinger, R., Sanli, I., Seeger, H., Tealeb, A., Toksöz, M.N., Veis, G. 2000. GPS constraints on plate motions and deformation in the Eastern Mediterranean: implications for plate dynamics. *Journal of Geophysical Research 105*, 5695–5719. https://doi.org/10.1029/1996JB900351

Mogi, K. 1962. Magnitude-frequency relation for elastic shocks accompanying fractures of various materials and some related problems in earthquakes. *Bulletin of the Earthquake Research Institute*, *Tokyo University* 40, 831–853.

Molchanov, O.A., Hayakawa, M., Oudoh, T., Kawai, E. 1993. Precursory effects in the subionospheric VLF signals for the Kobe earthquake. *Physics of the Earth and Planetary Interiors 105*, 239–248. https://doi.org/10.1016/S0031-9201(97)00095-2

Mousavi, S.M. 2017. Spatial variation in the frequency-magnitude distribution of earthquakes under the tectonic framework in the Middle East. *Journal of Asian Earth Sciences 147*, 193–209. https://doi.org/10.1016/j.jseaes.2017.07.040

Mulumulu, E., Polat, O., Chavez-Garcia, F.J. 2023. Ambient noise tomography of the Aegean region of Türkiye from Rayleigh wave group velocity. *Frontiers in Earth Science 11* (*1265986*), 1–12. https://doi.org/10.3389/feart.2023.1265986

Oral, M.B., Reilinger, R.E., Toksöz, M.N., Kong, R.W., Barka, A.A., Kınık, I., Lenk, O. 1995. Global positioning system offers evidence of plate motions in eastern Mediterranean. *EOS*, *Transactions American Geophysical Union 76* (*2*), 9–11. http:// dx.doi.org/10.1029/EO076i002p00009-01

Ormeni, R., Hasimi, A., Öztürk, S., Como, E. 2023. Correlations between seismic *b*-value and heat flow density in Vlora-Lushnja-Elbasani-Dibra Fault Zone in Elbasani area, central Albania. *Baltica 36* (*2*), 176–189. https://doi.org/10.5200/baltica.2023.2.7.

Öncel, A.O., Wilson, T.H. 2004. Correlation of seismotectonic variables and GPS strain measurements in western Turkey. *Journal of Geophysical Research 109* (*B11*), B11306. https://doi.org/10.1029/2004JB003101

Öncel, A.O., Wilson, T.H. 2007. Anomalous seismicity preceding the 1999 Izmit event, NW Turkey. *Geophysical Journal International 169* (*1*), 259–270. https://doi.org/10.1111/j.1365-246X.2006.03298.x

Över, S., Özden, S., Demirci, A., Gündoğdu, E. 2021. The inferences on the Aegean geodynamic context from 30 October 2020 Samos earthquake (Mw:6.8). *Tectonophysics 815* (*228998*), 1–15. https://doi.org/10.1016/j.tecto.2021.228998

Özer, Ç., Polat, O. 2017a. Local earthquake tomography of Izmir geothermal area, Aegean region of Turkey. *Bollettino di Geofisica Teorica ed Applicata 58* (*1*), 17–42. https://doi.org/10.4430/bgta0191

Özer, Ç., Polat, O. 2017b. 3-D crustal velocity structure of Izmir and surroundings. *Journal of the Faculty of Engineering and Architecture of Gazi University 32* (*3*), 733–747. https://doi.org/110.17341/gazimmfd.337620

Öztürk, S. 2015. A study on the correlations between seismotectonic *b*-value and *Dc*-value, and seismic quiescence *Z*-value in the Western Anatolian region of Turkey. *Austrian Journal of Earth Sciences 108* (*2*), 172–184, https://doi.org/10.17738/ajes.2015.0019

Öztürk, 2020. A study on the variations of recent seismicity in and around the Central Anatolian region of Turkey. *Physics of the Earth and Planetary Interiors 301* (*106453*), 1–11. https://doi.org/10.1016/j.pepi.2020.106453

Öztürk, S., Alkan, H. 2023. Multiple parameter analysis for assessing and forecasting earthquake hazards in the Lake Van region, Turkey. *Baltica 36* (*2*), 133–154. https://doi.org/10.5200/baltica.2023.2.4

Öztürk, S., Çınar, H., Bayrak, Y., Karslı, H., Daniel, G. 2008. Properties of the aftershock sequences of the 2003 Bingöl, M_D = 6.4, (Turkey) earthquake. *Pure and Applied Geophysics 165*, 349–371. https://doi.org/10.1007/s00024-008-0300-5

Peikert, J., Hampel, A., Bagge, M. 2023. Three-dimensional finite-element modeling of Coulomb stress changes on normal and thrust faults caused by pore fluid pressure changes and postseismic viscoelastic relaxation. *Geosphere 20* (*1*), 105–128. https://doi.org/10.1130/GES02672.1

Polat, O., Eyidoğan, H., Haessler, H., Cisternas, A., Philip, H. 2002. Analysis and interpretation of the aftershock sequence of the August 17, 1999, Izmit (Turkey) earthquake. *Journal of Seismology 6*, 287–306. https://doi.org/10.1023/A:1020075106875

Reilinger, R., McClusky, S., Vernant, P., Lawrence, S., Ergintav, S., Cakmak, R. 2006. GPS constraints on continental deformation in the Africa-Arabia-Eurasia continental collision zone and implications for the dynamics of plate interactions. *Journal of Geophysical Research 111 (B05411)*, 1–26. https://doi.org/10.1029/2005JB004051

Roy, S., Ghosh, U., Hazra, S., Kayal, J.R. 2011. Fractal dimension and b-value mapping in the Andaman-Sumatra subduction zone. *Natural Hazards 57*, 27–37. https://doi.org/10.1007/s11069-010-9667-6

Sboras, S., Lazos, I., Mouzakiotis E., Karastathis V., Pavlides, S., Chatzipetros, A. 2020. Fault modelling, seismic sequence evolution and stress transfer scenarios for the July 20, 2017 (*M*w 6.6) Kos-Gökova Gulf earthquake, SE Aegean. *Acta Geophysica 68*, 1245–1261. https://doi.org/10.1007/s11600-020-00471-8

Şaroğlu, F., Emre, Ö., Kuscu, I. 1992. Turkiye Aktif Fay Haritasi [Active Fault Map of Turkey]. *M.T.A. Publication, Ankara, Turkey* [In Turkish].

Scholz, C.H. 2015. On the stress dependence of the earthquake *b* value. *Geophysical Research Letters 42*, 1399–1402. https://doi.org/10.1002/2014GL062863

Schorlemmer, D., Wiemer, S., Wyss, M. 2005. Variations in earthquake-size distribution across dif-

ferent stress regimes. *Nature 437*, 539–42. https://doi.org/10.1038/nature04094

Sinaga, G.H.D., Silaban, W., Simanullang, A.F. 2022. Analysis of Coulomb stress of Sumatera earthquake against pyroclastic flow of mount Sinabung as data Prone Volcano disaster. *World Journal of Advanced Research and Reviews 13* (*1*), 793–803. https://doi.org/10.30574/wjarr.2022.13.1.0086.

Stein, R.S., King, G.C.P., Lin, J. 1994. Stress Triggering of the 1994 M = 6.7 Northridge, California, earthquake by its predecessors. *Science 265* (*5177*), 1432–1435. https://doi.org/10.1126/science.265.5177.1432

Şengör, A.M.C., Görür, N., Şaroğlu F. 1985. Strike-slip faulting and related basin formation in zones of tectonic escape: Turkey as a case study. *Society of Economic Paleontologists and Mineralogists. Special Publication 37*, 227–264. https://doi.org/10.2110/pec.85.37.0227

Tabban, A., Gencoğlu, S. 1975. Earthquake and its parameters. *Bulletin Earthquake Research Institute of Turkey 11*, 7–83.

Tan, O. 2021. A homogeneous earthquake catalogue for Turkey. *Natural Hazards and Earth System Sciences 21* (*7*), 2059–2073. https://doi.org/10.5194/nhess-21-2059-2021

Taymaz, T., Yolsal-Çevikbilen, S., Irmak, T.S., Vera, F., Liu, C, Eken, T., Zhang, Z., Erman, C., Keleş, D., 2022. Kinematics of the 30 October 2020 *Mw 7.0* N´eonKarlov´asion (Samos) earthquake in the Eastern Aegean Sea: Implications on source characteristics and dynamic rupture simulations. *Tectonophysics 826* (*229223*), 1–24. https://doi.org/10.1016/j.tecto.2022.229223

Toda, S., Stein, R.S., Richards-Dinger, K., Bozkurt, S.B. 2005. Forecasting the evolution of seismicity in southern California: animations built on earthquake stress transfer. *Journal of Geophysical Research: Solid Earth 110* (*B05S16*), 1–17. https://doi.org/10.1029/2004J B003415

Toda, S., Stein, R.S., Sevilgen, V., Lin, J. 2011. Coulomb 3.3 Graphic-rich deformation and stress-change software for earthquake, tectonic, and volcano research and teaching-user guide. U.S. *Geological Survey Open-File Report 2011–1060*, 63, available at https://pubs.usgs.gov/of/2011/1060/

Ulukavak, M., Yalçınkaya, M., Kayıkçı, E.T., Öztürk, S., Kandemir, R., Karslı, H. 2020. Analysis of ionospheric TEC anomalies for global earthquakes during 2000–2019 with respect to earthquake magnitude (Mw ≥ 6.0). *Journal of Geodynamics 135* (*101721*), 1–10. https://doi.org/10.1016/j.jog.2020.101721

Utsu, T. 1971. Aftershock and earthquake statistic (III): Analyses of the distribution of earthquakes in magnitude, time and space with special consideration to clustering characteristics of earthquake occurrence (1). *Journal of the Faculty of Science, Hokkaido University*, *Series VII* (*3*), 379–441.

Utkucu, M., Nalbant, S.S., Pınar, A., McCloskey, J., Nicbhloscaidh, M., Turhan, F., Yalçın, H., Kızılbuğa, S., Coşkun, Z., Ertan, E.K., Gülen, L. 2021. The June 12, 2017 M6. 3 Karaburun-Lesvos earthquake of the northern Aegean Sea: aftershock forecasting and stress transfer. *Tectonophysics 814* (*228945*). https://doi.org/10.1016/j.tecto.2021.228945

Wan, Y., Shen, Z-K. 2010. Static Coulomb stress changes on faults caused by the 2008 Mw 7.9 Wenchuan, China earthquake. *Tectonophysics 491*, 105–118. https://doi:10.1016/j.tecto.2010.03.017

Wessel, P., Luis, J.F., Uieda, L., Scharroo, R., Wobbe, F., Smith, W.H.F., Tian, D. 2019. The Generic Mapping Tools version 6. *Geochemistry Geophysics Geosystems 20*, 5556–5564. https://doi.org/10.1029/2019GC008515

Wiemer, S. 2001. A software package to analyze seismicity: ZMAP. *Seismological Research Letters 72* (*2*), 373–382. https://doi.org/10.1785/gssrl.72.3.373

Wiemer, S., Katsumata, K. 1999. Spatial variability of seismicity parameters in aftershock zones. *Journal of Geophysical Research 104* (*B6*), 13135–13151, https://doi.org/10.1029/ 1999JB900032

Wiemer, S., Wyss, M. 2000. Minimum magnitude of completeness in earthquake catalogs: Examples from Alaska, the Western United States, and Japan. *Bulletin Seismological Society of America 90* (*3*), 859–869. https://doi.org/10.1785/0119990114

Woessner, J., Wiemer, S. 2005. Assessing the quality of earthquake catalogues: Estimating the magnitude of completeness and its uncertainty. *Bulletin Seismological Society of America 95* (*2*), 684–698. https://doi.org/10.1785/0120040007

Yadav, R.B.S., Gahalaut, V.K., Chopra, S.B. 2012. Tectonic implications and seismicity triggering during the 2008 Baluchistan, Pakistan earthquake sequence. *Journal of Asian Earth Sciences 45*, 167–178. https://doi.org/10.1016/j.jseaes.2011.10.003

Yang, L., Wang, J., Xu, C. 2024. Coseismic Coulomb stress changes induced by a 2020–2021 MW > 7.0 Alaska earthquake sequence in and around the Shumagin gap and its influence on the Alaska-Aleutian subduction interface. *Geodesy and Geodynamics 15* (*1*), 1–12. https://doi.org/10.1016/j.geog.2023.04.007